Mechanics & Industry **21**, 504 (2020)
© AFM, EDP Sciences 2020
https://doi.org/10.1051/meca/2020057

Mechanics & Industry

Available online at:
www.mechanics-industry.org

Regular Article

The effect of NCG on the characteristics of hydraulic cavitation

Qiang Li*, Wei Li, Jian Zhang, Dezhi Ming, Weiwei Xu, and Zhenbo Wang

College of New Energy, China University of Petroleum (East China), Qingdao 266580, China

Received: 16 December 2019 / Accepted: 2 June 2020

Abstract. Hydraulic cavitation, as an important and complex hydrodynamic phenomenon, has long drawn attention. In this paper, the ZGB (Zwart-Gerber-Belamri) cavitation model is improved and the effect of NCG (noncondensable gas) on cavitation in water is studied by numerical simulation. The influence of NCG on the cavity length, the temperature of the cavities and the mixed viscosity of the cavities is investigated through the improved ZGB cavitation model. In addition, experiments on hydrodynamic cavitation produced by a Venturi tube are used to validate the improved ZGB cavitation model. The results show that NCG not only shortens the length of the cavity but also reduces the volume fraction of the vapor. The existence of NCG decreases the viscosity in the cavity of the Venturi tube but increases the viscosity at the sidewall of the tube. In addition, the temperature in the cavities increases with increasing NCG. Regardless of whether air is injected, the volume fraction of the vapor in the cavities increases first and then decreases with increasing temperature. However, the transition temperature decreases somewhat after injecting air. Therefore, the influence of NCG on hydraulic cavitation is significant, and the role of NCG should be considered in industry.

Keywords: Hydrodynamic cavitation / ZGB cavitation model / NCG / Venturi tube

1 Introduction

Hydraulic cavitation is a dynamic phase transition phenomenon that occurs when the local static pressure of liquid drops below the saturated vapor pressure [1]. This effect occurs in various fluid machinery, including turbines, pumps and marine propellers. When cavitation occurs, serious problems such as performance degradation, noise and vibration are often encountered in practice [2–6]. In the process of cavitation, many factors will cause the degree of cavitation, among which NCG in liquid will sometimes be ignored, but the NCG can change the characteristics of the fluid during cavitation, which has large effect on the performance of fluid machinery [7,8]. Therefore, it is necessary to explore the influence of NCG on hydraulic cavitation.

NCG has a significant influence on the characteristics of a fluid, such as the tensile strength of the liquid, the formation of bubbles, and the collapse and shedding of bubbles [9–11]. It was found that the presence of air can affect the initial volume of gas nuclei in liquid; thus, the tensile strength of liquids is changed [12]. Prosperetti et al. [13] found that the formation rate of cavitation bubbles is accelerated with increasing gas nuclei in water and finally reaches a constant value in the presence of NCG by the experimental method. Dharmadhikari [14] demonstrated that NCG significantly changes the dynamics of fluid collapse and that bubbles collapse sharply when the content of NCG exceeds 2%.

In the field of fluid machinery, the influence of NCG on the performance of hydraulic machinery is studied by means of experiment and numerical simulation. For the experimental investigation. Michele [15] found that NCG and turbulent disturbances had significant effects on cavitation in nozzle holes by means of numerical simulation and experiment. Wang et al. [16] studied the unsteady evolution of the ventilated cavitation of an axisymmetric vehicle, and the results showed that the amount of NCG volume has a significant effect on the shape of bubbles. Tang [17] found that the existence of NCG could lead to the deterioration of the heat transfer performance of machinery. Li [18] found that the increase in NPSHR in centrifugal pumps is related not only to the increase of viscosity but also to the increase in the volume fraction of NCG. Chirkov [19] and Kurzin [20] found that the cavitation generated during the operation of hybrid turbines produces strong self-excited pressure and power oscillation, and the injection of NCG can reduce the pressure fluctuation amplitude.

Numerical simulation has rapidly developed into an important method of studying hydraulic cavitation in recent years [21]. Charrière [22] studied periodic self-sustaining cavitation along a Venturi configuration by

* e-mail: liqiangsydx@163.com

numerical simulation. Deng [23] found by numerical simulation that the scale of the cavitation region and the vapor volume fraction in the pump are different when pumps transport different kinds of liquids, which is related to the viscosity and surface tension of the medium. Kadivar [24] proposed a passive control method based on cylindrical cavity generators (CCGs) on the base hydrofoil surface, and the influence of the passive controller on the dynamics of unsteady cloud cavitation was analyzed by numerical simulation.

The study of the characteristics of hydraulic cavitation inevitably involves the cavitation model. At present, the widely used cavitation models are the S–S cavitation model, ZGB cavitation model and full cavitation model. Schnerr and Sauer [25] proposed the S–S cavitation model, in which the mixture of water and vapor is seen as a mixture containing a large number of spherical vapor bubbles. The S–S model is widely applied in the numerical simulation of rotating machinery, such as centrifugal pumps. Zwart et al. [26] proposed the ZGB cavitation model by considering the influence of the density of gas nuclei in liquid on cavitation; they concluded that the increase of the vapor volume fraction in the cavity causes the decline of gas nuclei in liquid. To consider the effect of NCG on cavitation, Singhal et al. [27] presented a cavitation model incorporating NCG, which is called the full cavitation model. Moreover, many scholars have evaluated the numerical calculation of different cavitation models and improved individual cavitation models, which has brought the numerical results closer to the experimental data [28]. Liu [29] improved the S–S model and considered the influence of NCG, and the effect of eddy current on the cavitation of ALE15 hydrofoil was studied by numerical simulation. Hsiao et al. [30] and Ma et al. [31] proposed a multiscale cavitation model based on the Euler-Lagrange coupling method to capture the process of formation, development, collapse and cloud cavitation shedding. Zhao et al. [32] proposed the LVC cavitation model based on the ZGB cavitation model, which takes into account the effect of vortices on cavitation. The LVC cavitation model can reflect the length of vortices. Du et al. [33] proposed a new cavitation model based on the full cavitation model, taking the change of the amount and density of cavitation as an important factor.

The ZGB cavitation model converges more easily than the full cavitation model and is more suitable for Venturi tubes than the S–S cavitation model. Therefore, the ZGB cavitation model is improved in this paper, and the cavity in the Venturi tube is simulated. Based on the improved ZGB cavitation model, the effects of NCG on the cavity length, viscosity of the cavity and temperature of the cavity during cavitation are discussed.

2 Numerical simulation method

2.1 Governing equation

Assuming that the water phase and the vapor phase are fully mixed at all points in the flow field, the effect of the slip velocity between the liquid phase and the gas phase is neglected, and the transport equation of the mixture is solved directly. The continuum equation and momentum equation of the mixture composed of a water phase and a vapor phase are solved. The mixed continuity equation (1), momentum equation (2) and energy equation (3) are as follows:

$$\frac{\partial \rho_m}{\partial t} + \frac{\partial (\rho_m u_j)}{\partial x_j} = 0 \tag{1}$$

$$\frac{\partial (\rho_m u_i)}{\partial t} + \frac{\partial (\rho_m u_j u_i)}{\partial x_j} = -\frac{\partial p}{\partial x_i} + \frac{\partial}{\partial x_j}\left[(\mu_m + \mu_t)\left(\frac{\partial u_i}{\partial x_j} + \frac{\partial u_j}{\partial x_i} - \frac{2}{3}\frac{\partial u_k}{\partial x_k}\delta_{ij}\right)\right] \tag{2}$$

$$\frac{\partial (\rho_m E)}{\partial t} + \nabla[\vec{u}(\rho_m E + p)] = \nabla\cdot(k_{eff}\nabla T) \tag{3}$$

where ρ_m is the density of mixture phase, μ_m is the kinetic viscosity, μ_t is the turbulent viscosity coefficient and p is the local pressure. The subscripts (i, j, k) denote the directions of the Cartesian coordinates. Besides, E is the specific energy, expressed as $E = h - \frac{\rho}{\rho_m} + \frac{1}{2}|\vec{u}|^2$, where h is the enthalpy, and k_{eff} represents the effective thermal conductivity.

2.2 Turbulence model

Because the Reynolds number at the entrance of the flow field in the venturi is 37136.15, which is much larger than 4000. Therefore, turbulence model must be applied in this numerical simulation.

Yakhot and orzag proposed a RNG (Re-Normalization group) k–ε model based on the renormalization group method of the standard k–ε model [34,35]. The model has a better performance in cavitation numerical calculation because it adds an R term to the ε equation of turbulence dissipation rate and considers the swirling flow of turbulence [36,37]. So the equations are given here:

$$\frac{\partial}{\partial t}(\rho k) + \frac{\partial}{\partial x_j}(\rho k u_j) = \frac{\partial}{\partial x_j}\left[\left(\mu_m + \frac{\mu_t}{\sigma_k}\right)\frac{\partial k}{\partial x_j}\right] + P_t - \rho\varepsilon$$

$$\frac{\partial}{\partial t}(\rho\varepsilon) + \frac{\partial}{\partial x_i}(\rho\varepsilon u_i) = \frac{\partial}{\partial x_j}\left[\left(\mu_m + \frac{\mu_t}{\sigma_\varepsilon}\right)\frac{\partial \varepsilon}{\partial x_j}\right] + C_{1\varepsilon}P_t\frac{\varepsilon}{k} - C_{2\varepsilon}\rho\frac{\varepsilon^2}{k} - R \tag{4}$$

$$R = \frac{\eta(1-\eta/\eta_0)}{1+\beta\eta^3}\frac{\varepsilon}{k}P_t \tag{5}$$

$$\eta = \frac{Sk}{\varepsilon} \tag{6}$$

$$S = \sqrt{2\overline{S_{ij}}\,\overline{S_{ij}}} \tag{7}$$

$$\overline{S_{ij}} = \frac{1}{2}\left(\frac{\partial u_i}{\partial x_j} + \frac{\partial u_j}{\partial x_i}\right) \tag{8}$$

where $\boldsymbol{k}$ is the turbulent kinetic energy, $\boldsymbol{\varepsilon}$ is the turbulent dissipation rate, P_t is the turbulent kinetic energy generation term and t is the time. In these equations, $C_{1\varepsilon} = 1.42$, $C_{2\varepsilon} = 1.42$, $\sigma_k = 0.7179$, $\sigma_\varepsilon = 0.7179$, $\eta_0 = 4.38$, $\beta = 0.012$, $C_\mu = 0.085$.

2.3 Improved cavitation model

The effects of NCG on the fluid density, velocity, and pressure distribution cannot be ignored based on previous studies by Yang et al. [38]. Therefore, cavitation flow should be regarded as a mixture of liquid, vapor and NCG.

In general, the full cavitation model, S–S cavitation model and ZGB cavitation model are widely used in the calculation of cavitation flow. Comparing these three cavitation models, the disadvantage of the full cavitation model is that the convergence of numerical calculation is difficult in certain cases. The ZGB cavitation model and S-S cavitation model are more stable and convergent than the full cavitation model in the calculation process [39–41]. In addition, many scholars use the ZGB cavitation model to study cavitation in Venturi tubes [28]. From these points of view, the ZGB cavitation model is selected for this numerical calculation. However, the effect of NCG on cavitation flow has not been considered in the ZGB cavitation model. Thus, the ZGB cavitation model is improved, and the effect of NCG is considered in this paper.

It is generally known that the vapor volume fraction is the product of the number density of bubbles and the volume of a single bubble. Thus, the following eq is applied to express the volume fraction of the vapor:

$$\alpha_v = \rho_n \cdot \left(\frac{4}{3}\pi R_B^3\right) \tag{9}$$

where α_v depicts the volume fraction of vapor, ρ_n is the bubble number density, R_B is the radius of single bubble.

The total interphase mass transfer rate per unit volume is set as the product of the number density of bubbles and the mass of a single bubble (assuming that the bubble size is the same):

$$R_n = \rho_n \cdot \left(4\pi R_B^2 \rho_v \frac{DR_B}{Dt}\right) \tag{10}$$

where R_n is total interphase mass transfer rate per unit volume, ρ_v is the vapor phase density.

It should be noted that the ZGB cavitation model is based on the R–P (Rayleigh-Plesset) equation (11), which is used to describe the growth or collapse process of a single bubble under the action of internal and external pressure difference.

$$\frac{p_v - p}{\rho_l} = R_B\frac{D^2R_B}{Dt^2} + \frac{3}{2}\left(\frac{DR_B}{Dt}\right)^2 + \frac{4\nu_l}{R_B}\frac{DR_B}{Dt} + \frac{2S}{\rho_l R_B} \tag{11}$$

where p_v is the pressure in the bubble, ρ_l is the liquid phase density, ν_l is the kinematic viscosity of liquid phase, and S is the surface tension of the bubble.

Neglecting the influence of the second-order term, surface tension and liquid viscosity, the relationship between the change of bubble radius and pressure can be obtained:

$$\frac{DR_B}{Dt} = \pm\sqrt{\frac{2}{3}\frac{|p_v - p|}{\rho_l}}. \tag{12}$$

Substituting equations (9) and (12) into equation (10), the expression of the net mass transfer is shown as follows:

$$R_n = \frac{3\alpha_v\rho_v}{R_B}\sqrt{\frac{2}{3}\frac{p_v - p}{\rho_l}}. \tag{13}$$

The nucleation site density must decrease accordingly with increasing vapor volume fraction. To model this process, the Zwart-Gerber-Belamri model [27] is referred to in this paper, and the influence of NCG is considered as follows:

$$\begin{cases} R_e = F_v\dfrac{3\alpha_{\mathrm{nuc}}(1-\alpha_v-\alpha_g)\rho_v}{R_B}\sqrt{\dfrac{2}{3}\dfrac{p_v - p}{\rho_l}} & (p \le p_v) \\ R_c = F_c\dfrac{3\alpha_v\rho_v}{R_B}\sqrt{\dfrac{2}{3}\dfrac{p - p_v}{\rho_l}} & (p > p_v) \end{cases} \tag{14}$$

where R_e and R_c denote the vaporization and condensation rates per unit volume, respectively. F_v and F_c represent the evaporation coefficient and condensation coefficient per unit volume, which are empirical coefficients, for which Zwart et al. [27] recommend values of 50 and 0.01, respectively, following their extensive studies. α_g represents the volume of NCG. α_{nuc} depicts the nucleation site volume fraction. ρ_l is the density of liquid. Besides, p_v is the pressure in the bubble, which is expressed as follows:

$$p_v = p_{\mathrm{sat}} + 0.195\rho_m \cdot k \tag{15}$$

where p_{sat} represents the saturated vapor pressure of water. ρ_m represents density of mixture.

Because the mixture is composed of a liquid phase, vapor phase and NCG, the density of the mixture has been corrected as follows [34]:

$$\rho_m = \left[\alpha_v\rho_v + (1-\alpha_v-\alpha_g)\rho_l\right]/\left(1-f_g\right) \tag{16}$$

f_g is the mass fraction of NCG. The mass transferred through cavitation is modeled by the transport equation for

Table 1. The dimensions of each part of the model.

Serial number	Various parts	Dimension (mm)
1	Diameters at both ends	20
2	The length of contraction	15
3	The length of throat	10
4	The diameter of throat	5
5	The length of diffusion	75
6	Total length of Venturi tube	100

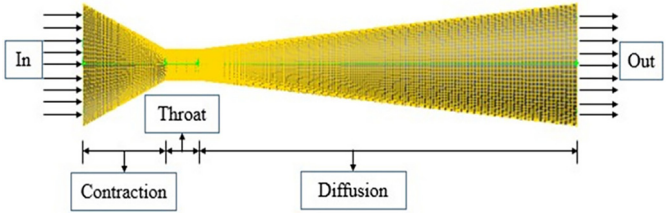

Fig. 1. The model of the Venturi tube.

the vapor mass fraction:

$$f_z = \alpha_z \frac{\rho_z}{\rho_m} (z = 1, 2, \ldots, n) \tag{17}$$

in which subscript z stands for the zth phase.

Generally, the saturated vapor pressure of water is set by default. For example, the saturated vapor pressure of water is 3540 Pa when the temperature is 298 K. In fact, the saturated vapor pressure of water vapor varies with temperature, so the saturated vapor pressure estimation is improved by incorporating the Antoine equation [42–44].

$$\log p_{\text{sat}} = A - B/(T - 273.15 + C) \tag{18}$$

where T represents the temperature. A, B and C are empirical parameters when the temperature ranges from 10 °C to 60 °C, and their values are 8.10765, 1750.286 and 235, respectively.

3 Numerical procedure

3.1 Model geometry

A Venturi tube can produce an obvious cavitation phenomenon. In addition, the pressure loss in the Venturi tube caused by flow is smaller than that in the orifice plate. Therefore, the influence of NCG has been studied based on the cavitation phenomenon of a Venturi tube. The dimensions of each part of the Venturi model are shown in Table 1, and the model of the Venturi tube is shown in Figure 1.

3.2 Boundary conditions and solution methods

The inlet pressure is set at 0.2 MPa, and the outlet pressure is atmospheric pressure at 0.1 MPa. The cavitation number

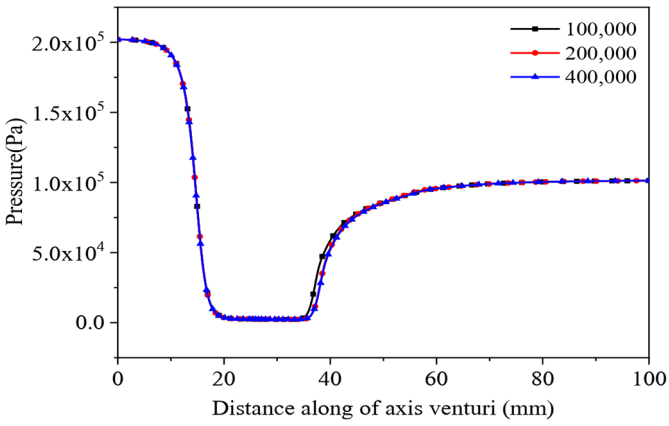

Fig. 2. Grid sensitivity analysis of the CFD simulation.

is $\sigma = 0.22$, defined $\sigma = (p_{ref} - p_v)/(0.5\rho l v^2)$, where v is the velocity of Venturi throat, p_{ref} is the reference pressure, p_v is the saturated vapor pressure of liquid, and ρ_l is the density of liquid phase. For the solution method of pressure, a linear discretization scheme is selected. For pressure–velocity coupling, the SIMPLE method is selected. Turbulent kinetic energy and turbulent energy dissipation rate are discretized as per second-order upwind discretization for improved accuracy.

CFD simulations are known to be sensitive to the mesh density. Therefore, the appropriate mesh density should be chosen to ensure the mesh quality. In this study, a sensitivity analysis was performed to ensure that the simulation results did not vary with the number of grids. The number of grids is 100,000, 200,000 and 400,000 for numerical calculation. The calculation results are shown in Figure 2. It can be seen that the pressure profiles do not vary significantly. A grid number of 200,000 is selected to ensure the quality of the grid and reduce the excess use of computing resources.

4 Results and discussion

The simulation requires comparative analysis through experiments to illustrate the reliability of the simulation, so a hydraulic cavitation experimental platform was built as shown in Figure 3. The platform consists of a thermal insulation water tank (volume = 35 L), turbine flowmeter, visualization test section (Venturi tube shown in Fig. 4), pressure transmitter (the accuracy of the pressure transmitter is 0.25% FS) and centrifugal pump (the flow rate is 2 m^3/h and the head of the pump is 20 m). The water flows out of the tank and is pumped to the experimental section of the visual venturi. At this point, cavitation is captured.

The numerical results were compared with the experimental results, including the outlet volume flow rate and the gray processing images of cavity distribution. Figure 5 shows a comparison of the outlet volume flow rates between the experiments and numerical simulations under different cavitation numbers. As shown in the figure, the numerical results are close to the experimental results,

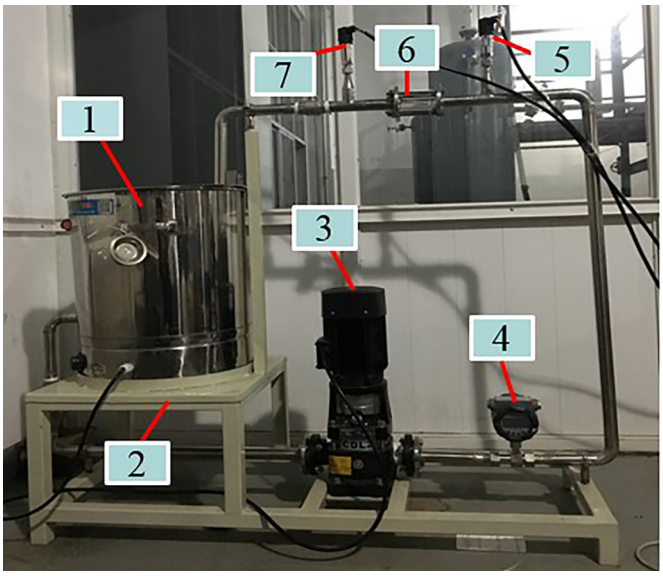

Fig. 3. Hydraulic cavitation test platform.

Fig. 4. Visual test section of the Venturi tube.

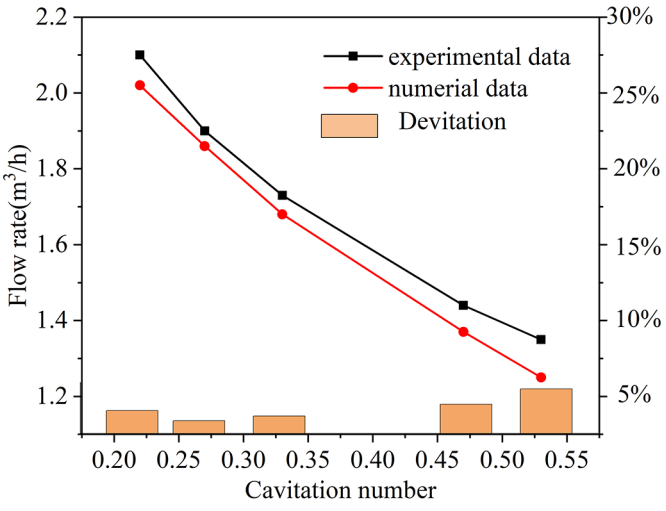

Fig. 5. Comparison of the outlet volume flow rate between numerical and experimental results.

the maximum deviation is about 5%. Also, for the cavitation number of 0.22 (the cavitation number selected for discussion in this paper), the deviation is 3.8%.

In addition, the cavity distribution in the diverging section of the Venturi tube is compared. The vapor volume fraction obtained by numerical result and the experimental result are shown in Figure 6. In addition, the same parts of simulation result and experimental result are cut off and grayed in Figure 6. Then, the gray value of the simulation result and six groups of experimental results are read after grayscale processing, as shown in Figure 7. Black indicates the presence of a cavity, and a gray area appears if bubbles collapse or disperse. Therefore, the more bubbles there are in a cavity, the darker the cavity appears. As illustrated in Figure 7, the axial location (X) is made dimensionless using the length of the diverging sect (L), and the diverging section is divided into five equal parts. It can be seen that the experimental results and simulation results show that when X/L is 0.25, the gray value is the minimum, that is, the volume fraction of vapor in the cavity reaches the maximum both in experiment and simulation. Therefore, the experimental results and simulation results are very consistent at this point and the simulation results are credible.

4.1 Effects of NCG on the cavity length

In general, the effect of NCG is not taken into account in the study of cavitation phenomena, which leads to some deviations in the simulation results. In this paper, the effects of six different contents of NCG on cavitation were analyzed. The contents of NCG were 0%, 0.5%, 1%, 2%, 4%, and 8%. The contours of the vapor volume fraction and the cavity are shown in Figure 8. It can be seen that cavitation begins at the start point of the throat of the Venturi tube, and the bubbles collapse at different locations at the diverging sect of the Venturi tube. To clarify the results, the contour of the vapor volume fraction simulated in the diverging sect of the Venturi tube is presented in grayscale, and the results are shown in Figure 9. The cavity length is shortened with the injection of NCG, as shown in both Figures 8 and 9.

Moreover, the maximum volume fraction of the vapor at the sidewall of the Venturi tube can reach 95% without NCG as shown in Figure 8, while the maximum volume fraction of the vapor at the sidewall of the Venturi tube can be reduced to approximately 85% when air is injected. Therefore, the existence of NCG weakens the cavitation intensity and shorten the length of the cavitation cavity.

In fact, bubbles grow on the wall. Cavitation begins when the pressure of the flow field falls below the saturated vapor pressure. Most vapor bubbles grow on the wall of the equipment without air. Only water and gas nuclei exist in the flow field if air is not injected. When air is injected, there are three components of water, gas nuclei and NCG in the flow field, and the nucleation site volume fraction in the ZGB model is constant. As a result, the number of gas nuclei in the water decreases, as does the number of bubbles produced in the process of cavitation, which leads to the shortening of the bubble length.

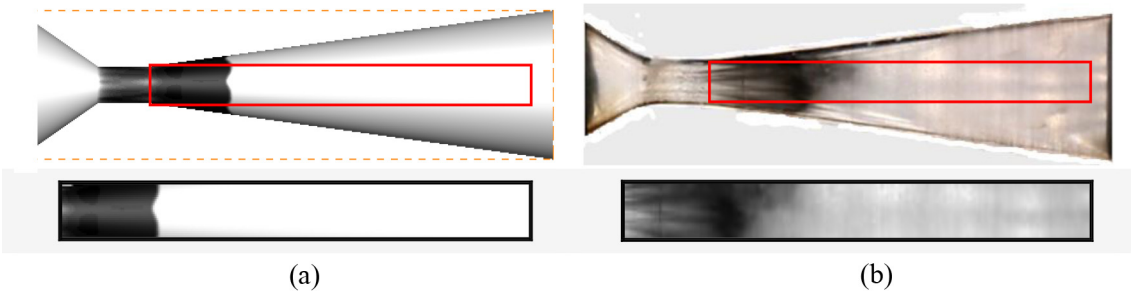

Fig. 6. Gray Processing of Simulated and Experimental Results. (a) numerical result (NCG 0.5%). (b) experimental result.

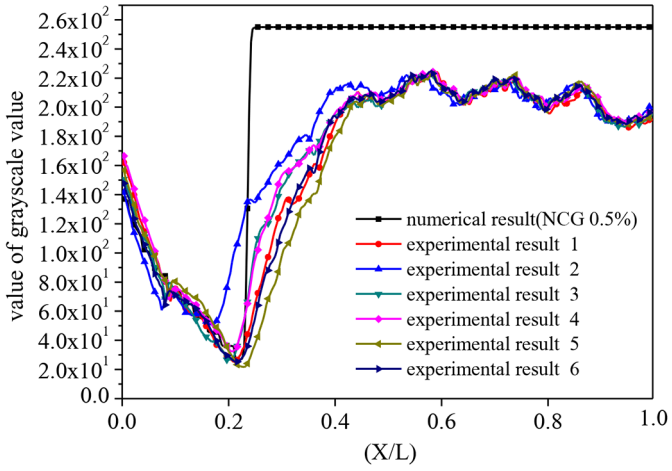

Fig. 7. Comparisons between experimental results and the simulation results. (Comparing the simulated results with the six experimental results by grayscale processing in terms of the tendency of cavitation.)

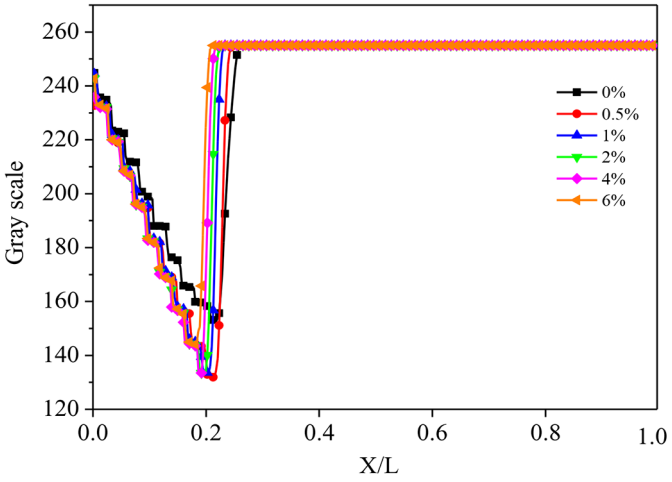

Fig. 9. Comparison of gray values between the simulation results of the vapor volume fraction with different contents of NCG.

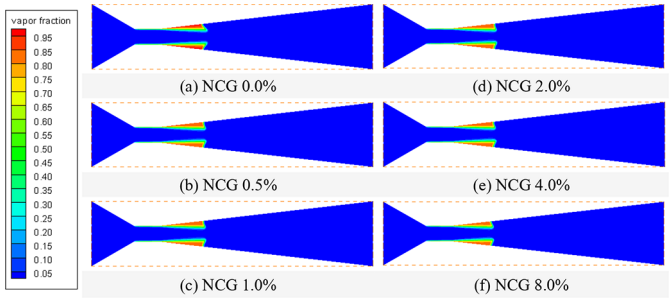

Fig. 8. Volume fraction of the vapor with different amounts of NCG on the plane of symmetry.

4.2 Effects of NCG on the viscosity of the mixed flow

To obtain the effect of the NCG on the viscosity, the viscosity of the mixture on the axis of the centerline and the sidewall of the Venturi tube was extracted to plot the curves shown in Figure 10. The viscosity of the mixture at the center of the cavity is the highest when NCG is 0, as shown in Figure 10a. It can be shown that the viscosity of the mixture decreases obviously with increasing NCG during cavitation. This result is due to the quite low viscosity of air itself, which is similar to that of vapor. Therefore, the viscosity of the mixture composed of air, vapor and water further decreases in the cavity.

However, the viscosity of the mixture in the cavity at the wall is the lowest when the content of NCG is 0, as shown in Figure 10b. This result occurs because the volume fraction of the vapor decreases with the injection of air, as shown in Figure 11. Therefore, a larger number of vapor bubbles are generated on the wall without NCG. Moreover, the formation of vapor bubbles further reduces the viscosity of the mixture.

4.3 Effects of NCG on the temperature during cavitation

To explore the influence of different NCG contents on the temperature in the cavity, the NCG contents were set to 0%, 0.5%, 1.0%, 2.0%, 4%, and 8%. It can be seen that the temperature in the cavity decreases when NCG is not injected, as shown in Figure 12. This result arises because when cavitation occurs, the gas nucleus absorbs heat from the fluid and begins to grow, which leads to a decrease in the temperature in the cavity. The temperature in the cavity decreases from 298 K to 288 K, a difference of 10 K, when NCG is not injected. However, the temperature

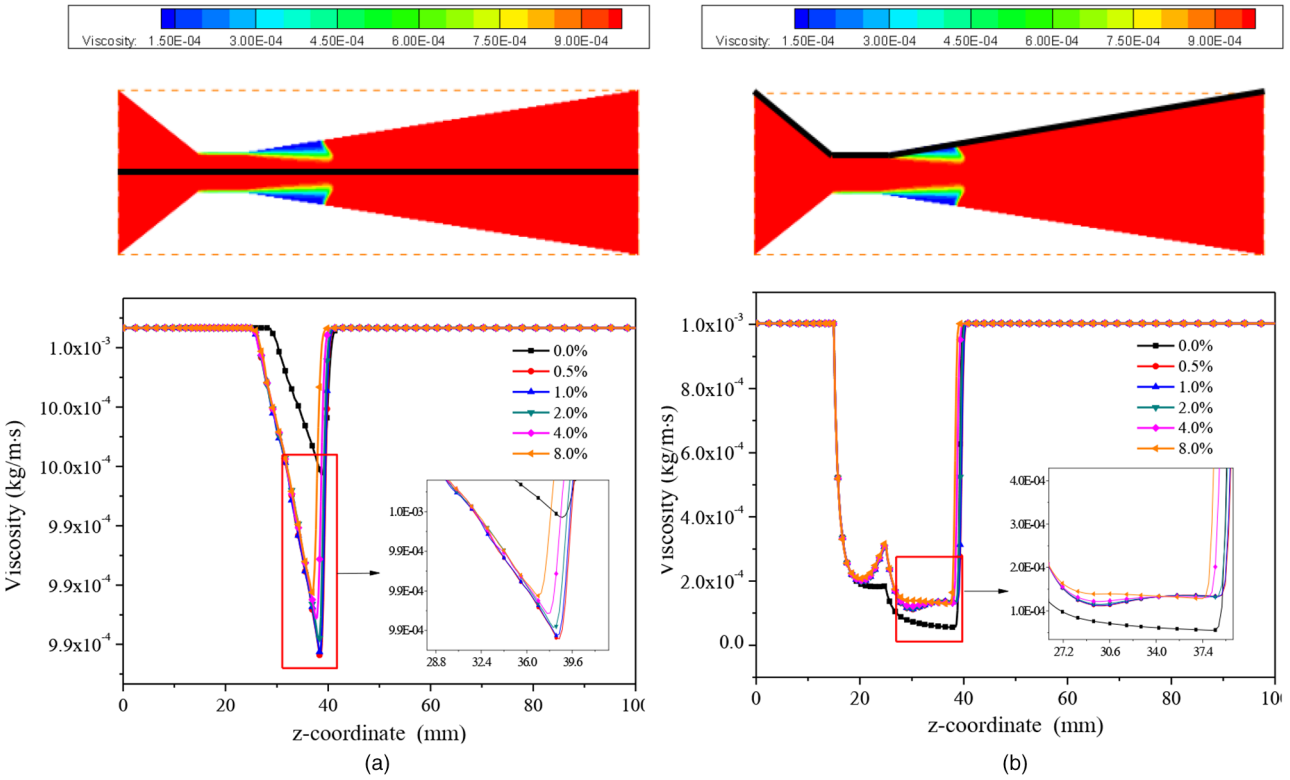

Fig. 10. Viscosity with different contents of NCG. (a) Viscosity distribution on centerline. (b) Viscosity distributionnear the wall.

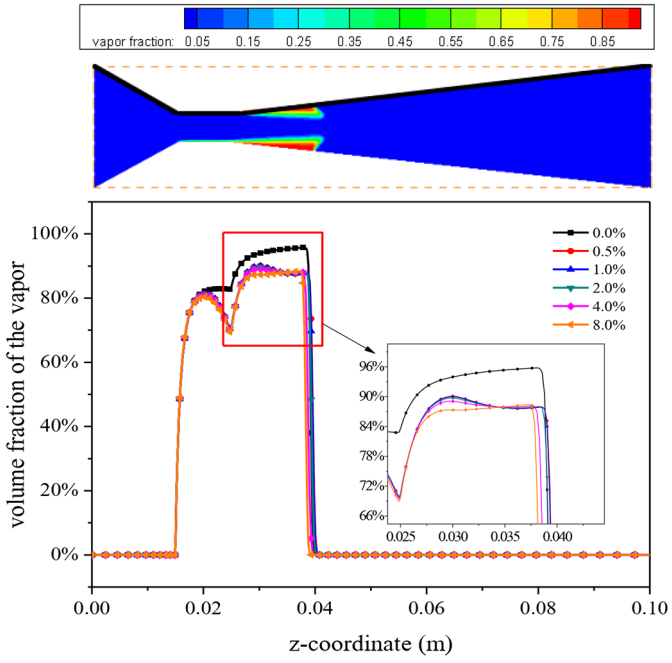

Fig. 11. Volume fraction of the vapor near the wall of the Venturi tube with different amounts of NCG.

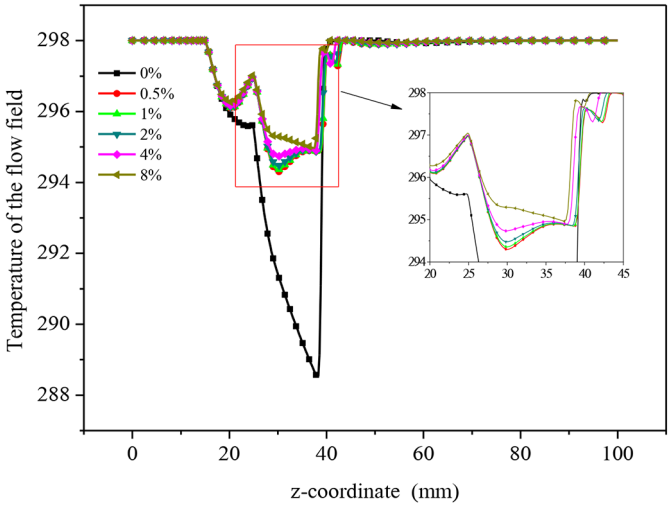

Fig. 12. Temperature of the Venturi tube near the wall of the tube with different NCG contents.

decreases from 298 K to 294 K, a difference of 4 K, when NCG is injected. Therefore, the attenuation amplitude of temperature in the cavity with NCG is much lower than that without NCG. This result can be attributed to the volume fraction of the liquid phase decreasing due to the NCG and the volume fraction of the nucleation site being fixed, which leads to a decrease in the number of gas nuclei in the water. Therefore, the heat absorbed by the gas nuclei growth is reduced, and the temperature in the cavity of the Venturi tube decreases during cavitation. In addition, the temperature increases with increasing NCG content, which coincides with the effect of NCG on the cavity length.

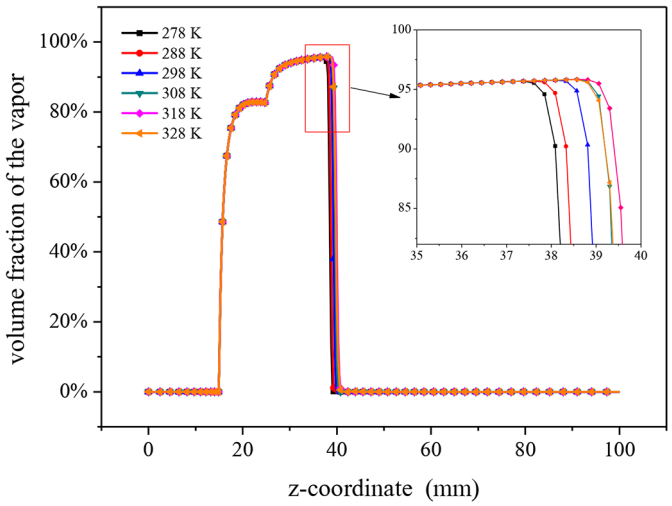

Fig. 13. Volume fraction of the vapor near the wall of the Venturi tube with different temperatures without NCG.

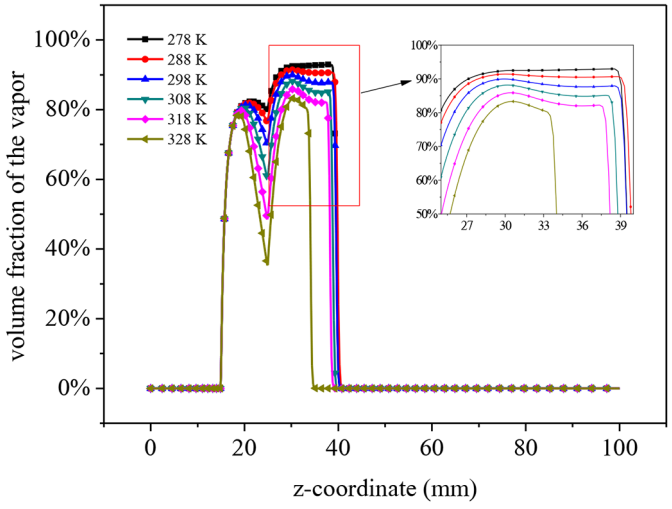

Fig. 14. Volume of the vapor near the wall of the Venturi tube with different temperatures when the NCG content is 1%.

To explore the influence of NCG on cavitation at different temperatures, the temperatures were set to 278 K, 288 K, 298 K, 308 K, 318 K, and 328 K. First, when the NCG content is 0, the result is as shown in Figure 13. It can be seen that the volume fraction of the vapor behaves essentially the same as the temperature increase. The cavity length first increases and then decreases. The transition point is 318 K. This result occurs because when the temperature increases, the saturated vapor pressure increases, which is more likely to cause cavitation. However, the pressure in the bubble increases, and the buffer effect is enhanced when the bubbles are close and the temperature is too high, which weakens the cavitation.

The situation is different when the NCG content is 1%. Though the cavity length first increases and then decreases with increasing temperature, the transition point is 288 K, as shown in Figure 14. There are two main reasons. On the one hand, because NCG expands with increasing temperature and the volume fraction of water in the flow field decreases, the number of gas nuclei decreases. Therefore, the cavity length is shortened rapidly. On the other hand, the increasing temperature causes the rapid expansion of gas nuclei in the water, thus causing a sustained increase in the liquid pressure in the flow field, which accelerates the collapse of the vapor bubbles.

5 Conclusion

In this paper, a physical model of a Venturi tube is established, and the ZGB cavitation model is improved for numerical calculation. The effects of NCG on the characteristics of the flow field are calculated based on the improved ZGB cavitation model. The validity of the research method is illustrated by a self-built experimental platform.

The conclusions drawn from the study can be summarized as follows:

- The existence of NCG affects the cavity length in cavitation. The length of the cavity decreases with increasing NCG content, and the volume fraction of the vapor also decreases with the injection of NCG.
- The viscosity at the center of the cavity decreases after NCG is injected. In contrast, the viscosity of the mixture on the wall of the cavity increases with increasing NCG.
- The temperature in the cavity increases with increasing NCG.
- It can be seen that the temperature in the cavity decreased from 298 K to 288 K, a difference of nearly 10 K. However, the temperature dropped from 298 K to 294 K after injecting NCG, a difference of 4 K.
- The cavity length first increases and then decreases with increasing temperature when the content of NCG is 0%. The transition temperature is 318 K. The transition temperature decreases from 318 K to 288 K when the NCG content is 1%.

Nomenclature

h	Thermal entropy ($J \cdot mol^{-1} \cdot K^{-1}$)
k_{eff}	Effective thermal conductivity ($W \cdot m^{-1} \cdot K^{-1}$)
P_t	Turbulent kinetic energy generation term
P	The local pressure (Pa)
t	Time (s)
R_B	The radius of single bubble (m)
R_n	The total interphase mass transfer rate per unit volume
P_V	The pressure in bubble (Pa)
R_e	The vaporization rate per unit volume
R_c	The condensation rate per unit volume
F_v	The evaporation coefficient per unit volume
F_c	The condensation coefficient per unit volume
P_{sat}	Liquid saturation vapor pressure (Pa)
f_g	The mass fraction of NCG

T	The temperature (K)
$\boldsymbol{k}$	Turbulent kinetic energy ($m^2 s^{-2}$)
A,B,C,$C_{1\varepsilon}$,$C_{2\varepsilon}$,σ_k, σ_ε,η_0,β,C_μ	Empirical parameters
p_{ref}	The reference pressure (Pa)
v	The velocity of venture throat ($m \cdot s^{-1}$)

Greek symbols

ρ_m	The density of mixture phase (kg/m^3)
μ_m	Kinetic viscosity ($N \cdot s/m^2$)
μ_t	Turbulent viscosity coefficient
ν_m	The velocity of mixture phase ($m \cdot s^{-1}$)
α_v	The volume fraction of vapor
ρ_n	Bubbles number density (kg/m^3)
ρ_V	The vapor phase density (kg/m^3)
α_g	The volume of gas0
α_{nuc}	The nucleation site volume fraction
ρ_l	The density of liquid phase (kg/m^3)
ε	The turbulent dissipation rate ($m^2 s^{-3}$)

Dimensionless number

σ Cavitaition number

Subscripts

i,j,k The directions of the Cartesian coordinates

This work is supported by the National Natural Science Foundation of China (51506225), the Key Research and Development Program of Shandong, China (2018GHY115018), the Fundamental Research Funds for the Central Universities (18CX02129A).

References

[1] F.R. Young, Cavitation, Acoust. Soc. Am. **91**, 3591 (1992)
[2] B.K. Ahn, T.K. Lee, H.T. Kim et al., Experimental investigation of supercavitating flows, Int. J. Nav. Archit. Ocean Eng. **4**, 123–131 (2012)
[3] E. Roohi, M.R. Pendar, A. Rahimi, Simulation of three-dimensional cavitation behind a disk using various turbulence and mass transfer models, Appl. Math. Model. **40**, 542–564 (2016)
[4] M.R. Pendar, E. Roohi, Investigation of cavitation around 3D hemispherical head-form body and conical cavitators using different turbulence and cavitation models, Ocean Eng. **112**, 287–306 (2016)
[5] E. Kadivar, O. el. Moctar, K. Javadi, Investigation of the effect of cavitation passive control on the dynamics of unsteady cloud cavitation, Appl. Math. Model. **72**, 716–716 (2019)
[6] D. Yang, Y.L. Xiong, X.F. Guo, Drag reduction of a rapid vehicle in supercavitating flow, Int. J. Nav. Archit. Ocean Eng. **9**, 35–44 (2017)
[7] M.J. Braun, W.M. Hannon, Cavitation formation and modelling for fluid film bearings: a review, Proc. Inst. Mech. Eng. J. **224**, 839–863 (2010)
[8] D. Sun, S.Y. Li, C.W. Fei et al., Investigation of the effect of cavitation and journal whirl on static and dynamic characteristics of journal bearing, J. Mech. Sci. Technol. **44**, 1305–1320 (2019)
[9] G.D.C. Kumar, V.A. Kumar, R.K. Gupta et al., Effect of strain rate and temperature on the tensile flow behavior and microstructure evolution in Fe-0.3 Pct C-CrMoV grade steel, Metall. Mater. Trans. A **50A**, 161–171 (2019)
[10] V.G. Baidakov, V.E. Vinogradov, Limiting stretchings of liquid oxygen: experiment and classical nucleation theory, Int. J. Heat Mass Transf. **129**, 1057–1065 (2019)
[11] Q.S. Yan, G. Lu, G.M. Luo et al., Effect of synergistic action of ultrasonic vibration and solidification pressure on tensile properties of vacuum counter-pressure casting aluminum alloy, China Foundry **15**, 411–417 (2018)
[12] L.J. Briggs, Limiting negative pressure of water, J. Appl. Phys. **21**, 721–722 (1950)
[13] A. Prosperetti, Vapor bubbles, Annu. Rev. Fluid Mech. **49**, 221–248 (2017)
[14] A.K. Dharmadhikari, J.A. Dharmadhikari, A.V. Mahulkar et al., Dynamics of photothermally created vaporous, gaseous, and mixed microbubbles, J. Phys. Chem. C **115**, 6611–6617 (2011)
[15] M. Battistoni, D.J. Duke, A.B. Swantek et al., Effects of NCGes and turbulent fluctuations on cavitation phenomenon in injector nozzle, Atom. Sprays **25**, 453–483 (2015)
[16] Y.W. Wang, C.G. Huang, X. Fang et al., Characteristics of the re-entry jet in the cloud cavitating flow over a submerged axisymmetric projectile, Chin. J. Hydrodyn. **28**, 23–29 (2013)
[17] J. Tang, C. Yan, L.C. Sun, Effects of NCG and ultrasonic vibration on vapor bubble condensing and collapsing, Exp. Therm. Fluid Sci. **61**, 210–220 (2015)
[18] W.G. Li, Effects of viscosity on turbine mode performance and flow of a low specific speed centrifugal pump, Appl. Math. Model. **40**, 904–926 (2016)
[19] D.V. Chirkov, P.K. Shcherbakov, S.G. Cherny et al., Numerical investigation of the air injection effect on the cavitating flow in Francis hydro turbine, Thermophys. Aeromech. **24**, 691–703 (2017)
[20] V.B. Kurzin, Model for the formation of acoustic self-oscillations in a chamber with a jet flowing through its nozzle, J. Appl. Mech. Technol. Phys. **58**, 1040–1052 (2017)
[21] B. Ji, H.Y. Cheng, B. Huang et al., Research progresses and prospects of unsteady hydrodynamics characteristics for cavitation, Adv. Mech. **49**, 201906 (2019)
[22] B. Charriere, E. Goncalves, Numerical investigation of periodic cavitation shedding in a Venturi, Int. J. Heat Fluid Flow **64**, 41–54 (2017)
[23] S.S. Deng, G.D. Li, J.F. Guan et al., Numerical study of cavitation in centrifugal pump conveying different liquid materials, Results Phys. **12**, 1834–1839 (2019)
[24] E. Kadivar, O. el. Moctar, K. Javadi, Stabilization of cloud cavitation instabilities using cylindrical cavitating-bubble generators (CCGs), Int. J. Multiph. **115**, 108–125 (2019)
[25] G.H. Schnerr, J. Sauer, Physical and numerical modeling of unsteady cavitation dynamics, in *Fourth International Conference on Multiphase Flow, New Orleans*, 2001
[26] P.J. Zwart, A.G. Gerber, T. Belamri, A two-phase flow model for predicting cavitation dynamics, in *Fifth International Conference on Multiphase Flow, Yokohama*, 2004

[27] A.K. Singhal, H.Y. Li, M.M. Athavale et al., Mathematical basis and validation of the full cavitation model, J. Fluids Eng. Trans. ASME **124**, 617–624 (2002)
[28] W. Li, Y.F. Yang, W.D. Shi et al., The correction and evaluation of cavitation model considering the thermodynamic effect, Math. Probl. Eng. **2018**, 1–11 (2018)
[29] M. Liu, L. Tan, S. Cao, Cavitation–vortex–turbulence interaction and one-dimensional model prediction of pressure for hydrofoil ale15 by large eddy simulation, J. Fluids Eng. Trans. ASME **142**, 062013 (2019)
[30] C.T. Hsiao, J.S. Ma, G.L. Chahine, Multiscale tow-phase flow modeling of sheet and cloud cavitation, Int. J. Multiph. Flow. **90**, 102–117 (2017)
[31] J.S. Ma, C.T. Hsiao, G.L. Chahine, A physics based multiscale modeling of cavitating flows, Comput. Fluids **145**, 68–84 (2017)
[32] Y. Zhao, G. Wang, B. Huang, A cavitation model for computations of unsteady cavitating flows, Acta. Mech. Sin. **32**, 273–283 (2016)
[33] T.Z. Du, Y.W. Wang, L.J. Liao et al., A numerical model for the evolution of internal structure of cavitation cloud, Phys. Fluids **28**, 077103 (2016)
[34] V. Yakhot, S.A. Orszag, Renormalization group analysis of turbulence. I. Basic theory[J], J. Sci. Comput. **1**, 3–51 (1986)
[35] V. Yakhot, S.A. Orszag, S. Thangam et al., Development of turbulence models for shear flows by a double expansion technique, Phys. Fluid Fluid Dyn. **4**, 1510 (1992)
[36] W.D. Shi, G.J. Zhang, D.S. Zhang, Evaluation of turbulence models for the numerical prediction of transient cavitation around a hydrofoil, IOP Conf. Ser. Mater. Sci. Eng. **52**, 062013 (2013)
[37] L. Zhou, Z. Wang, Numerical simulation of cavitation around a hydrofoil and evaluation of a RNG k-ε model, J. Fluids Eng. Trans. ASME **130**, 011302 (2008)
[38] Q. Yang, Y. Wang, Z. Zhang, Scale effects on propeller cavitating hydrodynamic and hydroacoustic performances with non-uniform inflow, Chin. J. Chem. Eng. **26**, 414–426 (2013)
[39] A. Iannetti, M.T. Stickland, W.M. Dempster, A CFD and experimental study on cavitation in positive displacement pumps: Benefits and drawbacks of the 'full' cavitation model, Eng. Appl. Comp. Fluid Mech. **10**, 57–71 (2016)
[40] A. Iannetti, M.T. Stickland, W.M. Dempster, An advanced CFD model to study the effect of non-condensable gas on cavitation in positive displacement pumps, in *11th international symposium on compressor & turbine flow systems theory & application areas SYMKOM 2014. IMP2, Lodz*, 2014
[41] A. Iannetti, M.T. Stickland, W.M. Dempster, A computational fluid dynamics model to evaluate the inlet stroke performance of a positive displacement reciprocating plunger pump, Proc. Inst. Mech. Eng. A **28**, 574–584 (2014)
[42] D. Roizard, Antoine Equation[M]// Encyclopedia of Membranes, 2016
[43] J. Wisniak, Historical development of the vapor pressure equation from dalton to Antoine, J. Phase Equ. Diffus. **22**, 622–630 (2001)
[44] W. Wagner, New vapour pressure measurements for argon and nitrogen and a new method for establishing rational vapour pressure equations, Cryogenics **13**, 470–482 (1973)

Cite this article as: Q. Li, W. Li, J. Zhang, D. Ming, W. Xu, Z. Wang, The effect of NCG on the characteristics of hydraulic cavitation, Mechanics & Industry **21**, 504 (2020)